

Automatic Diagnosis of Carotid Atherosclerosis Using a Portable Freehand 3D Ultrasound Imaging System

Jiawen Li, Yunqian Huang, Sheng Song, Hongbo Chen, Junni Shi, Duo Xu, Haibin Zhang, Man Chen*, Rui Zheng*

Abstract— Objective: The objective of this study is to develop a deep-learning based detection and diagnosis technique for carotid atherosclerosis using a portable freehand 3D ultrasound (US) imaging system. **Methods:** A total of 127 3D carotid artery datasets were acquired using a portable 3D US imaging system. A U-Net segmentation network was firstly applied to extract the carotid artery on 2D transverse frame, then a novel 3D reconstruction algorithm using fast dot projection (FDP) method with position regularization was proposed to reconstruct the carotid artery volume. Furthermore, a convolutional neural network was used to classify the healthy case and diseased case qualitatively. 3D volume analysis including longitudinal reprojection algorithm and stenosis grade measurement algorithm was developed to obtain the clinical metrics quantitatively. **Results:** The proposed system achieved sensitivity of 0.714, specificity of 0.851 and accuracy of 0.803 respectively in diagnosis of carotid atherosclerosis. The automatically measured stenosis grade illustrated good correlation ($r=0.762$) with the experienced expert measurement. **Conclusion:** The developed technique based on 3D US imaging can be applied to the automatic diagnosis of carotid atherosclerosis. **Significance:** The proposed deep-learning based technique was specially designed for a portable 3D freehand US system, which can provide carotid atherosclerosis examination more conveniently and decrease the dependence on clinician's experience.

Index Terms—3D ultrasound imaging, automatic carotid atherosclerosis diagnosis, carotid artery segmentation, reconstruction with regularization.

I. INTRODUCTION

CAROTID atherosclerosis is one of the major causes of stroke which is the world's second leading cause of death [1]. The prevalence rate of carotid atherosclerosis is 36.2% in Chinese people over 40 years old [2]. The pathological features of carotid atherosclerosis are increase of intima-media thickness and appearance of atherosclerosis plaque. Magnetic resonance imaging (MRI), computed tomography angiography

This work was sponsored by Natural Science Foundation of China (NSFC) under Grant No.12074258. (Jiawen Li and Yunqian Huang are co-first authors.) (Corresponding authors: Rui Zheng, Man Chen.)

Jiawen Li, Sheng Song, Duo Xu and Haibin Zhang are with School of Information Science and Technology, ShanghaiTech University, Shanghai, China.

Hongbo Chen is with School of Information Science and Technology, ShanghaiTech University, Shanghai 201210, China, also with Shanghai Advanced Research Institute, Chinese Academy of Sciences, Shanghai 200050,

(CTA) and digital subtraction angiography (DSA) are several commonly used methods for visualizing and characterizing carotid artery features [3]–[5]. However, these methods still have some limitations during application due to invasiveness, ionizing radiation, heavy equipment etc.; and the approaches are very time-consuming and expensive which can't satisfy the need of large scale of examinations in different environments especially for community and countryside areas. 2D Ultrasound (US), as a non-invasive and low-cost method, is widely used in the examination of carotid plaque. However, there are several disadvantages of traditional 2D US in the current ultrasound examination of carotid atherosclerosis. (1) It is mainly carried out by experienced sonographers in hospital, and becomes a huge burden for health care system. (2) Routine health check is difficult for carotid atherosclerosis patients especially in rural or undeveloped area. (3) Routine ultrasound examination is a tedious, laborious, experience-dependent work for sonographers. (4) Clinically, some metrics such as intima-media thickness (IMT), plaque thickness, plaque area, usually assess the severity of the carotid atherosclerosis in 2D US images, which is prone to variability and lack of 3D morphology of carotid plaque [6], [7]. 3D US carotid artery imaging approaches mainly include mechanical scanning and tracked freehand scanning using various sensors e.g., magnetic tracked sensor, optical tracked sensor, etc., [8] which can provide plaque volume estimation, 3D morphology of plaque and other 3D metrics for carotid atherosclerosis diagnosis. The 3D techniques are found to be more accurate to evaluate the progress of carotid atherosclerosis [9]–[12]. Therefore, it is of great importance to develop a portable, reliable and cost-effective automatic ultrasound diagnostic technique for carotid atherosclerosis screening.

The automatic diagnosis of carotid atherosclerosis focuses on finding the biomarkers on the ultrasound images, for example

China, and also with University of Chinese Academy of Sciences, Beijing 100049, China.

Yunqian Huang and Junni Shi are with Tongren Hospital, Shanghai Jiao Tong University School of Medicine, Shanghai, China.

Man Chen is with Tongren Hospital, Shanghai Jiao Tong University School of Medicine, Shanghai, China (e-mail: maggiech1221@126.com)

Dr. Rui Zheng is with School of Information Science and Technology, Shanghai Engineering Research Center of Energy Efficient and Custom AI IC, ShanghaiTech University, Shanghai, China (phone: 86 21-2068 4452, e-mail: zhengrui@shanghaitech.edu.cn)

vessel wall area, vessel wall volume or total plaque volume [13]–[15]. These biomarkers are all bounded by the two boundaries of vessels, the media-adventitia boundary (MAB) and the lumen-intima boundary (LIB), thus identifying these two boundaries is an important issue during the carotid atherosclerosis diagnosis. In recent years, deep learning methods have achieved excellent performance in medical image processing. Jiang *et al.* [16]–[18] designed a novel adaptive triple loss for carotid artery segmentation. To utilize 3D information in 3D volume of carotid artery, Jiang *et al.* [19] introduced a fusion module to the U-Net segmentation network and yielded promising performance on carotid segmentation task. Zhou *et al.* [20] proposed a deep learning-based MAB and LIB segmentation method, and a dynamic convolutional neural network (CNN) were applied to image patches in every slice of the 3D US images. LIB segmentation was performed by U-Net based on the masks of the MAB since the LIB is inside the MAB. The method achieved high accuracy but initial anchor points were still manually placed. Ruijter *et al.* [21] created a generalized method to segment LIB using CNN. Several U-Nets were compared and the experiments showed that the combination of various vessels such as radial, ulnar artery, or cephalic vein improved the segmentation performance of carotid artery. After segmentation, a 3D-geometry can be obtained for further therapy. Van Knippenberg *et al.* [22] proposed an unsupervised learning method to solve the lack of data in carotid segmentation task. Azzopardi *et al.* [23] designed a novel geometrically constrained loss functions and received improved segmentation results. Zhou *et al.* [24] proposed a voxel based 3D segmentation neural network to segment the MAB and LIB in 3D volume directly. Although the proposed algorithm achieved high accuracy with fast process, user's interaction is yet required to identify ROI in the first and last slice of the volume.

After region of interest (ROI) i.e., carotid artery is identified, further analysis needs to be performed to get significant clinical information for carotid atherosclerosis diagnosis such as the existence of plaque, carotid stenosis grade, type of the plaque, etc. Zhou *et al.* [25], [26] applied 8 different backbone and UNet++ segmentation algorithm trained on 2D longitudinal US images to segment the plaque region and calculate the total plaque area. Xia *et al.* [27] employed a CNN to categorize segmented carotid images into normal cases, thickening vessel wall cases and plaque cases. Ma *et al.* [28] proposed a multilevel strip pooling-based convolutional neural network to investigate the echogenicity of plaque which was found to be closely correlated with the risk of stroke. Shen *et al.* [29] proposed a multi task learning method, the authors combined ultrasound reports and plaque type label to train a CNN to classify four different plaque type. Zhao *et al.* [30] utilized a novel vessel wall thickness mapping algorithm to evaluate the therapeutical performance on carotid atherosclerosis. Zhou *et al.* [31] utilized the unsupervised pretrained parameters of U-Net to train a plaque segmentation network with a small 3D carotid artery ultrasound dataset. Saba *et al.* [32] used a deep learning based method to measure the carotid stenosis, three deep learning based systems were evaluated on 407 US dataset, and achieved

AUC of 0.90, 0.94 and 0.86 on the longitudinal US images respectively. Biswas *et al.* [33] proposed a two-stage artificial intelligence model for jointly measurement of atherosclerotic wall thickness and plaque burden in longitudinal US images. The results showed that the proposed method achieved the lowest error compared to previous method.

The current 3D carotid imaging device was mainly based on mechanical system and hard to transport which was almost impossible to apply in community or rural area, therefore the portable freehand 3D ultrasound imaging system was required which can be easily applied for various scenarios. However, for the freehand 3D ultrasound reconstruction, the requested small voxel size and various noise would lead to reconstruction artifacts [34], [35]. On the other hand, the clinicians in different scenarios were usually inexperienced so that the diagnosis results might be inaccurate and hard to reproduce compared with sonographers in clinical ultrasound department. In this paper, we developed a new detection and classification technique based on deep-learning algorithms for carotid atherosclerosis diagnosis which can be employed to a portable freehand 3D US imaging system for fast screening. Compared to other 3D ultrasound carotid artery imaging methods mainly focusing on carotid vessel wall segmentation [18], [20], [21], [24], the proposed method aimed at exploring an automatic and experience-independent technique and framework for fast carotid arteriosclerosis diagnosis.

The main contributions are outlined as follows. Firstly, a portable freehand 3D US carotid imaging and diagnosis framework including deep-learning based segmentation, 3D reconstruction and automatic volume analysis was developed for fast carotid atherosclerosis diagnosis. Secondly, a novel position regularization algorithm was designed to reduce the reconstruction error caused by freehand scan. Lastly, post analysis including automatic reprojection and stenosis measurement from 3D volume data provided visible qualitative results and quantitative results for atherosclerosis diagnosis.

II. METHODS

Fig. 1 showed the overview of data processing procedure including transverse image segmentation, 3D volume reconstruction, detection of carotid atherosclerosis and 3D carotid volume analysis.

A. MAB and LIB Segmentation

Three consecutive frames were concatenated in channel dimension which is proved to be useful to improve the segmentation accuracy [36].

Since the adjacent frames contained lots of redundant information, the pseudo labels were generated using pseudo-labeling method to reduce the work load [37]. One of every 5 neighbor frames were selected to be manually labeled by experienced sonographers and the other four frames were inferred by the network which was trained using the labeled frames. All generated pseudo labels were checked visually, the labels would be corrected if the segmentation is incorrect.

The intensity of the image was normalized to [0,1] as follows:

$$I = \frac{I - I_{min}}{I_{max} - I_{min}} \quad (1)$$

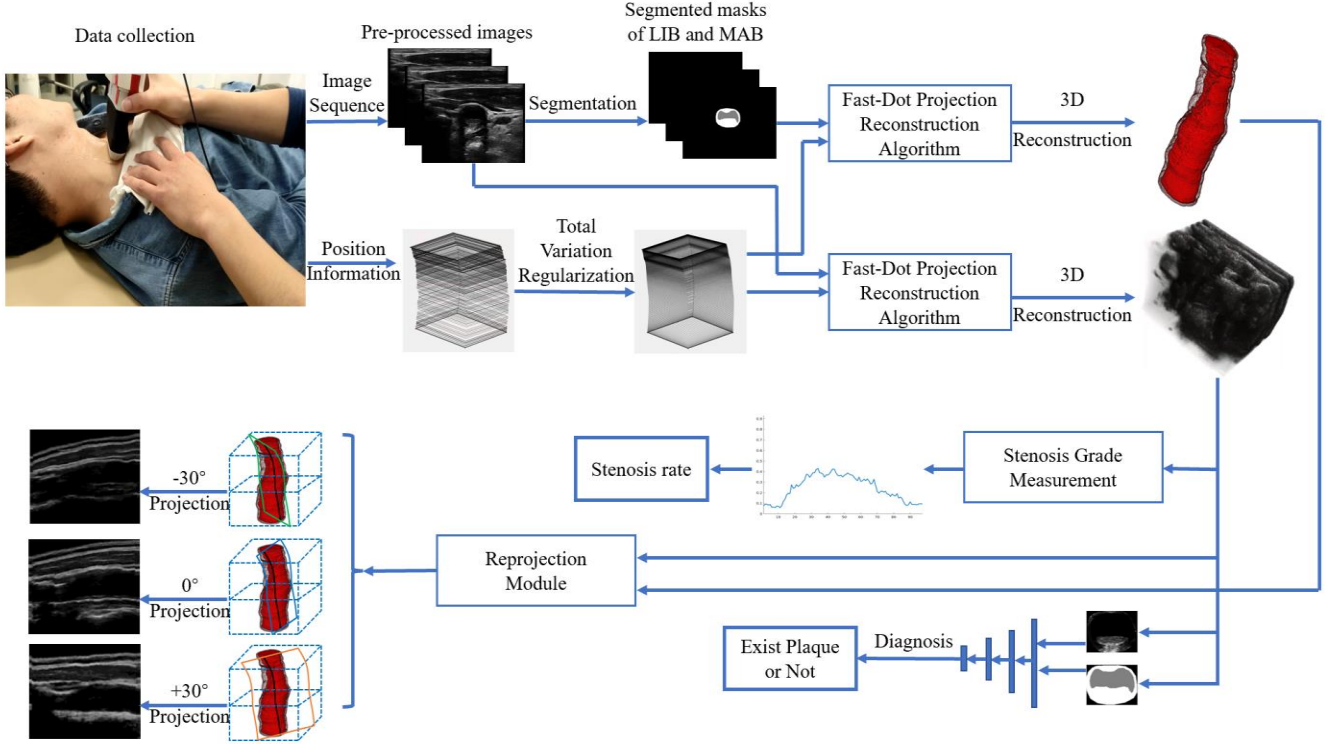


Fig. 1. The pipeline of the proposed system and corresponding algorithm. The top row demonstrated the process of the data acquisition, extraction of ROI and 3D reconstruction. The bottom row represented the process of 3D carotid volume analysis. The original image sequence and corresponding position information were firstly obtained by the 3D US device. U-Net segmentation algorithm and regularized Fast-Dot Projection algorithm was applied to extract the ROI and 3D carotid volume. Then 3D carotid volume analysis included automatic stenosis grade measurement, longitudinal image reprojection and healthy/diseased cases classification was conducted based on the reconstructed volume.

where I represented the intensity of the image. I_{\max} and I_{\min} represent the max and minimum value of the intensity in the US image. All images and corresponding labels were resized to 224*224 for segmentation network training.

U-Net was employed to segment the MAB and LIB in the transverse US image sequence [38]. The architecture of the network was illustrated in Fig. 2. The segmentation module consisted of two symmetrical sub-module which were encoder and decoder. The number of channels for each convolutional layer were set to (64, 128, 256, 512, 512). Each convolutional layer was followed by a batch normalization module and a

rectification linear unit (ReLU) module. The two modules were connected using skip connection to exploit all resolution features. The loss function of the segmentation module was the combination of DSC loss and cross-entropy loss:

$$Loss = Loss_{dice} + Loss_{ce} \quad (2)$$

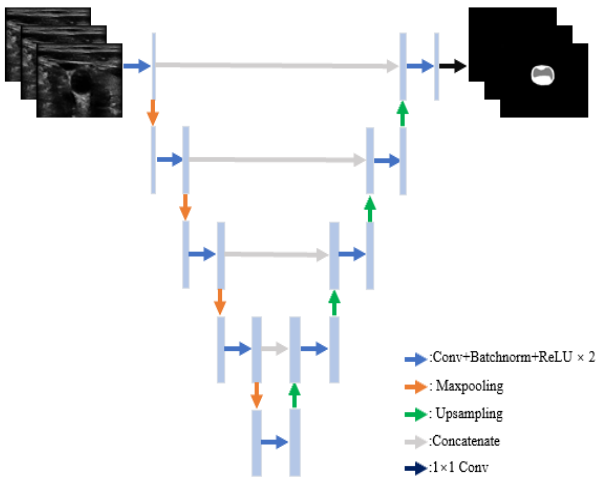
B. 3D Reconstruction with Regularization

After the MAB and LIB were identified in every slice of US image sequence, the 3D carotid artery volume was reconstructed using the Fast Dot Projection (FDP) method [39]. However, some disturbances caused by the low precision of the magnetic sensor, inevitable hand shaking and breathing movement during carotid swept, would lead to the reconstruction errors and artifacts. The major problem was the repeated acquisition at the same or very close positions, and it caused large uncertainty at volume voxels and discontinuity in the reconstructed volume [40]. To improve the image quality and decrease the uncertainty of 3D reconstructed volume, a total variation regularization [41] method was integrated with FDP reconstruction algorithm.

(1) For all the position information obtained from 3DUS device, it could be formulated as a set of rotation matrix R and a translation t . The tuple (R, t) consisting of all R and t formed the special Euclidean group $SE(3)$ which was the semi-direct product of the rotation group $SO(3)$ and the translation group. Therefore, the $SE(3)$ can be formulated as:

$$SE(3) = \left\{ \begin{pmatrix} R & t \\ 0 & 1 \end{pmatrix} : R \in SO(3), t \in \mathbb{R}^3 \right\} \quad (3)$$

Fig. 2. The architecture of the segmentation module.



(2) The position signal obtained by the 3DUS system could be considered as a set of entries which forms a vector $\mathbf{P} = (\mathbf{p}_1, \mathbf{p}_2, \dots, \mathbf{p}_k) \in M^k$, where k was the number of entries and $k \in N$, M^k was a manifold and $M = SE(3)$. Another signal set \mathbf{X} were considered to be found when the following formula is minimal.

$$E(\mathbf{x}) = D(\mathbf{x}, \mathbf{p}) + \alpha R(\mathbf{x}), \alpha > 0 \quad (4)$$

Where $D(x, p)$ was the penalizing term to reduce the variation between original signal \mathbf{P} and resulted signal \mathbf{X} . $R(\mathbf{x})$ was a regularized term to penalize the position saltation in the signal \mathbf{X} .

(3) The deviation penalized term $D(x, p)$ could be defined as:

$$D(\mathbf{x}, \mathbf{f}) = \sum_{i=1}^k (h \circ d)(\mathbf{x}_i, \mathbf{p}_i) \quad (5)$$

Where $d(\mathbf{x}_i, \mathbf{p}_i)$ was the length of the geodesic which was defined as a shortest path on M between two pose \mathbf{p} and \mathbf{q} [41]. h was defined as following:

$$h(s) = \begin{cases} s^2, & s < 1/\sqrt{2} \\ \sqrt{2}s - 1/2, & \text{otherwise} \end{cases} \quad (6)$$

Which was the Huber-Norm.

(4) For the regularized term, it could be defined as the following:

$$R(\mathbf{x}) = \sum_{i=1}^{k-1} (h \circ d)(\mathbf{x}_i, \mathbf{x}_{i+1}) \quad (7)$$

Where $d(\mathbf{x}_i, \mathbf{x}_{i+1})$ could be considered as the first-order forward difference. The optimize problem in (4) could be solved using a cyclic proximal point algorithm.

However, the original regularized algorithm couldn't handle the scanning positions with large backward movements. In this case, the position array was not sequential according to the coordinates, therefore pose re-rank algorithm was proposed. Concretely, considering the centroid point of every frame from the 2D segmented image sequence as $\mathbf{C}_k = (\mathbf{c}_1, \mathbf{c}_2, \dots, \mathbf{c}_k)$, the PCA (principal components analysis) algorithm was conducted in \mathbf{C}_k and a new matrix D_k was obtained. The first column of the matrix was the principal vector v_k , then a set of vectors \mathbf{c}_d could be acquired by projecting every centroid vector \mathbf{c}_k to v_k .

$$\mathbf{c}_d = \mathbf{c}_k - \frac{\mathbf{c}_k \cdot v_k}{v_k \cdot v_k} v_k \quad (8)$$

The new position sequence was finally obtained by sorting the 12-norm of the \mathbf{c}_d set.

C. Carotid Atherosclerosis Diagnosis

The US scans including the segmented and reconstructed volume were classified into healthy case and carotid atherosclerosis case using a diagnosis network. As illustrated in Fig. 3, there were two inputs for the diagnosis module. It had been proved that the morphological information was helpful for the network to classify the normal or abnormal (diseased) image [42], therefore the mask of LIB and MAB extracted from each slice of the reconstructed volume was used as one input. The other input was the cropped ROI which was determined by the max bounding rectangular of the mask, and in the cropped image, the intensity in the region between LIB and MAB was set to the original value, while the region inside lumen and outside vessel wall were set to 0. For each input stream, it consisted of three repeated blocks, each block consisted of two

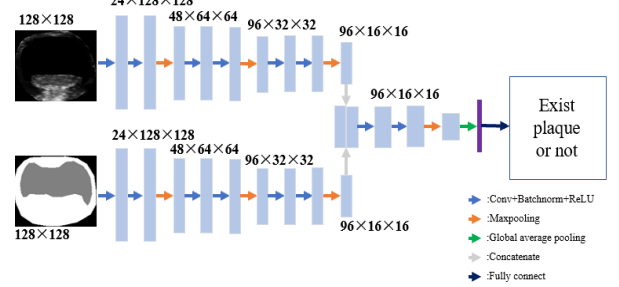


Fig. 3. The architecture of the diagnosis module.

consequent basic convolutional sub-block and a max pooling layer. The basic convolutional sub-block was composed of a convolutional layer, a batch normalization module and a linear rectification unit. The number of channels for each repeated block were set to (24, 48, 96). The fusion block concatenated the high-level features of two streams and combined information by introducing a basic convolutional sub-block. After fusion block, the remaining layers were global average pooling (GAP) layers and a fully connected layer to output the diagnosis result. We used focal loss in the diagnosis module.

The scan would be diagnosed as a carotid atherosclerosis case if the consecutive 5 transverse slices from the reconstructed volume were classified as existing plaque.

D. 3D Carotid Volume Analysis

The clinical diagnostic parameters such as plaque thickness, plaque length, stenosis grade, plaque area, plaque type, etc. can be directly calculated from the reconstructed carotid artery volume. To validate accuracy of the proposed method, the longitudinal US images of carotid artery were obtained by projecting the volume in different angles, and the stenosis grade was calculated.

Stenosis rate was usually used to evaluate the stenosis grade. For the slices which were diagnosed as atherosclerosis, stenosis degree can be evaluated using the LIB and MAB masks. The diameter stenosis rate was usually calculated to evaluate the stenosis grade in clinic. We denote it as

$$S_{diameter} = \frac{L_{wall}}{L_{wall} + L_{lumen}} \quad (9)$$

where L represented the length of respective area. The metric was ranged from 0 to 1, the greater number indicated the more severe stenosis. The length of vessel wall L_{wall} and length of

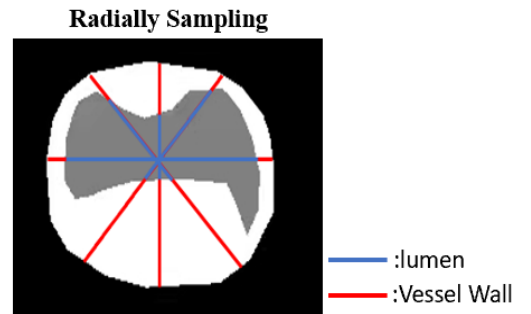


Fig. 4 The illustration of the approach to calculate the diameter stenosis.

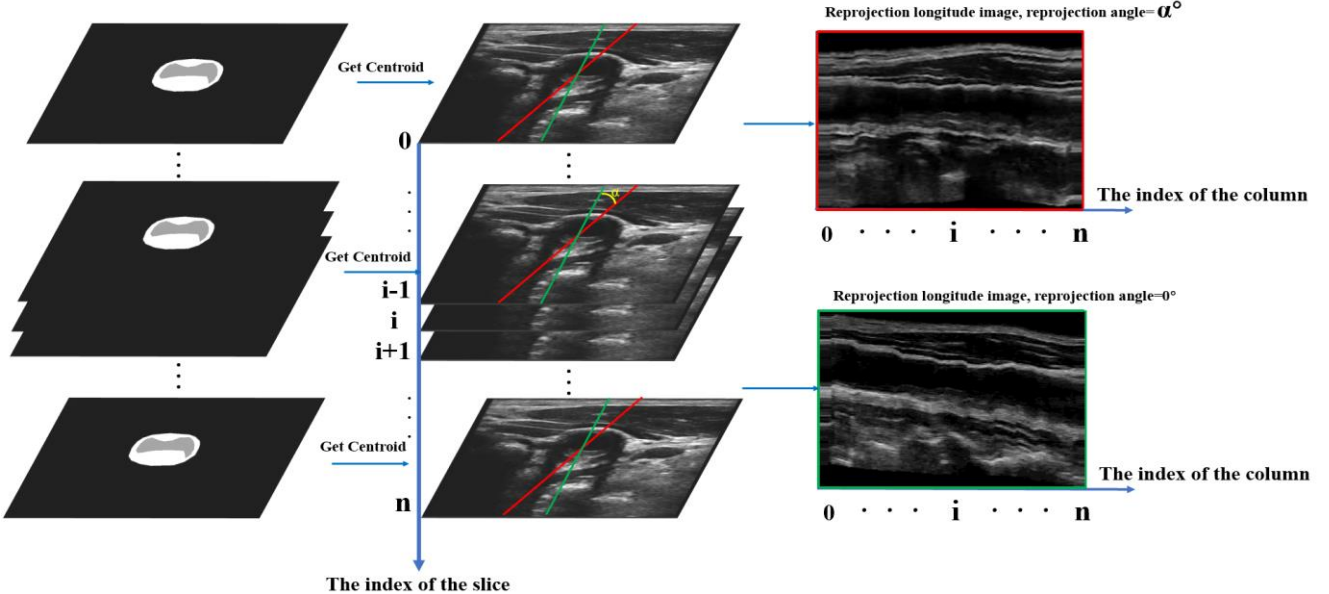


Fig. 5. The illustration of the reprojection process. The centroid point was calculated by the segmented MAB mask for each slice in the volume. Then the line segment crosses the centroid point was set to conduct the reprojection. The red and green line segment represent the different resample angle respectively.

lumen L_{lumen} were illustrated as Fig. 4. The diameter stenosis rate was the max $S_{diameter}$ which was calculated using all points in MAB boundary.

The longitudinal carotid US images were usually used to calculate plaque size and evaluate the morphology of plaque. Since the carotid artery is curved volume, the direct projection along a fixed axis may lead to missing of some structure. Therefore, centroid points of carotid artery in transverse slices were selected to determine the projection plane. Specifically, as illustrated in Fig. 5, denoting the centroid point of i -th slice in the volume as C_i , the line which was θ degree angled with y-axis through the centroid point C_i , was sampled as the i -th column of projected longitude image. In our experiment, the longitudinal US images were obtained by reprojecting the 3D carotid volume at the angles of 0° , $\pm 15^\circ$ and $\pm 30^\circ$.

III. EXPERIMENTAL SETUP

A. Data Acquisition and 3D Ultrasound Scan

A portable freehand 3D ultrasound imaging system was used to obtain three-dimensional images of carotid artery as shown in Fig. 6. The system consisted of a 2D linear probe (Clarius, L738-K, Canada), an electromagnetic tracking system (Polhemus, G4 unit, U.S.A) and a host laptop computer (Intel i7-8700k CPU @ 3.70GHz, 32GB RAM) [43]. The 2D transverse US images were acquired by the probe while the corresponding position and orientation information were captured by the magnetic sensor. The images and orientation were acquired with a frame rate of 24 Hz.

During the acquisition, the subjects took the supine position and was scanned as shown in Fig. 6 (d), and the probe swept consistently along the long axis of common carotid artery from the proximal end to the distal end at the speed of approximate 10-15 seconds per scan. To reduce the reconstruction artifacts, fallback along the swept direction and large movement normal to the swept direction should be avoided. The inclusion criteria

were based on visible plaques which was identified by expert. The stenosis grade larger than 70% was excluded to the dataset.

A total of 127 3D carotid artery scans from 83 subjects with stenosis range from 0% to 70% were obtained from local hospital, and all subjects consented to participate in this experiment, which was approved by the local ethics committee. The age of the subjects was ranged from 51 to 86 years old (Male: 38, Female: 45).

Each scan contained 122-250 2D transverse US images with resolution of 640*480. 7596 2D images from 40 scans were manually delineated for MAB and LIB and labeled for healthy or diseased (with plaque) by experienced sonographers for further training of segmentation and classification network. All

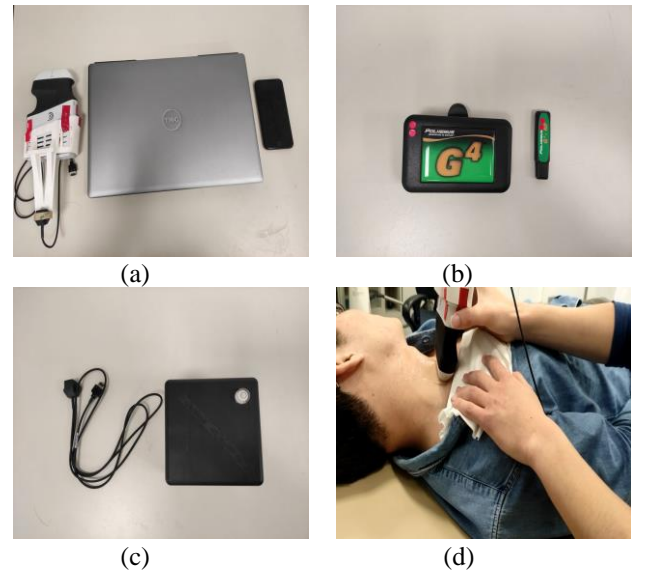


Fig. 6. Ultrasound scan using the freehand imaging system. (a) a handheld US scanner (left), a host laptop computer (middle) and an iPhone SE2 (right). (b) Tracking system including a hub (left) and a RF/USB module (right). (c) The sensor (left) and the magnetic source (right). (d) Ultrasound scan using the freehand imaging system.

127 scans were labeled for healthy or diseased (with plaque) by the same raters examining 2D images. In addition, stenosis grade and plaque size of randomly selected 20 scans were manually measured by expert using clinical 2D US device for verification of the proposed system and algorithm.

B. Training Methods

25 scans (4694 2D images) were randomly chosen for CNN training and 15 scans (2362 2D images) for validation in order to build and verify the segmentation module. The original images were resized to 224*224. All training process were performed using Pytorch 1.5.1 and Python 3.7 on a NVIDIA RTX 4000 GPU. The two networks were trained separately. For the segmentation module, the applied data augmentation strategies including gamma transformation, rotation, zoom, horizontal and vertical flip, and Adam optimizer were used. The network was trained for 100 epochs with learning rate and batch size set to 0.005 and 8 respectively. For the diagnosis module, the cropped and resized 2D US image segmented with the mask and the corresponding vessel wall mask were used for network training. Gamma transformation and horizontal & vertical flip were applied for data augmentation. The diagnosis network was trained for 50 epochs using Adam optimizer with learning rate and batch size set to 0.005 and 64 respectively.

C. Diagnosis parameter measurement

To verify the regularized reconstruction and longitudinal images reprojection algorithm, the longitudinal images from 20 clinical patients with and without regularization were compared with clinical images acquired by experienced sonographers visually, and the projection angles were set as $\theta = -30^\circ, -15^\circ, 0^\circ, 15^\circ, 30^\circ$.

The plaque length and thickness were manually measured on the 3D pseudo volume, the reconstructed 3D volume and the clinical images acquired by experienced sonographers respectively, where 3D pseudo volume was the volume which were stacked directly by the 2D US images sequence. The manual measurement of plaque length and thickness was conducted on the reprojected longitudinal images, among which the reprojection angle was chosen based on the carotid structural integrity and maximum stenosis grade. For plaque size measurement in reprojected image of reconstructed 3D volume, the pixel size was $0.2 \times 0.2 \text{ mm}^2$. For the pseudo 3D volume, the velocity of the swept was assumed constant, therefore the pixel size of reprojected image was determined by the distance of the swept which could be calculated by the magnetic sensor.

The whole system in clinical metric measurement was also verified by comparing stenosis rate automatically measured by the system and manually measured by experienced sonographers using clinical US device on 20 random clinical atherosclerosis patients according to formula (9).

D. Evaluation Metrics and Statistic Analysis

The dice similarity coefficient (DSC) and 95% hausdorff distance (HD95) were used to evaluate the performance of the carotid sequence segmentation. DSC indicated the quantitative metric of the overlap region between the ground truth and prediction mask which was defined as follows:

$$DSC = \frac{2(P \cap L)}{P \cup L} \quad (10)$$

where P, L were the prediction mask and ground truth. The hausdorff distance was defined as Eq (11), which indicated the largest point-wise matching discrepancy:

$$HD(A, B) = \max(hd(A, B), hd(B, A)) \quad (11)$$

where

$$hd(A, B) = \max_{a \in A} (\min_{b \in B} \|a - b\|) \quad (12)$$

$$hd(B, A) = \max_{b \in B} (\min_{a \in A} \|b - a\|) \quad (13)$$

For the evaluation of the diagnosis module. The specificity, sensitivity and accuracy were calculated for both 2D US image and scans.

The mean absolute difference (MAD) and standard deviation (SD) between results from the pseudo/reconstructed 3D volumes and results from experienced sonographers were investigated. The metrics in verification of the system, i.e., the stenosis grade, were compared between manual or automatic approach using the proposed technique and manual measurement using the clinical US device with the Pearson correlation analysis.

IV. RESULTS

A. Segmentation and Diagnosis Accuracy

The comparison between nine typical segmented images from U-Net and experienced sonographers was illustrated as Fig. 7, and the images were selected from different scans at some specific locations. Table I showed the average DSC and HD95 between the ground truth and prediction results.

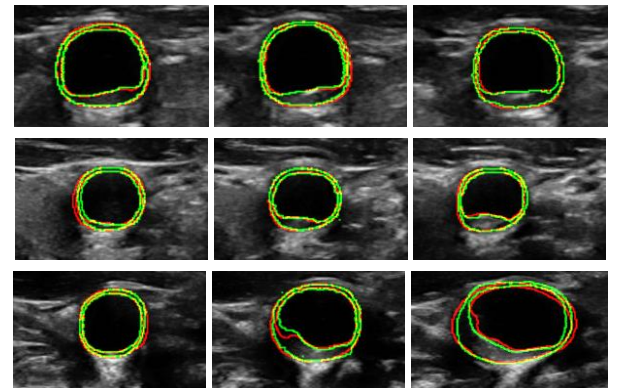


Fig. 7. Comparison of the auto segmentation from U-net (red) and manual segmentation from ground truth (green).

TABLE I. THE RESULTS OF VESSEL SEGMENTATION

Metrics	category	
	<i>MAB</i>	<i>Lumen</i>
DSC	95.00%	93.30%
HD95(pixel)	4.34	4.65

Table II showed the contingency table of the validation set of 2362 2D transverse images, and the sensitivity, specificity and accuracy were 0.73, 0.97 and 0.91 respectively. Table III showed the diagnostic results of carotid atherosclerosis for all

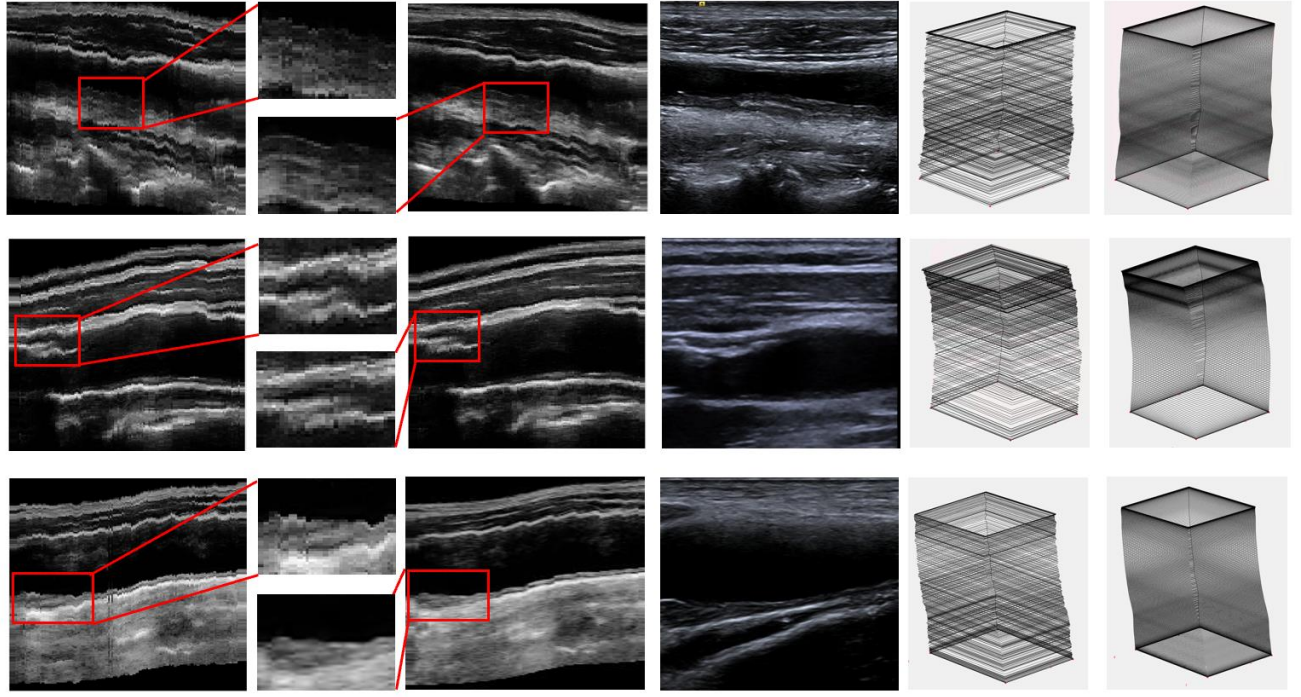


Fig. 8. Illustration of the US longitudinal images and the corresponding orientation information from three carotid atherosclerosis patients (by rows). The images in the first column were reconstructed without regularization algorithm while the images in the third column were reconstructed with regularization algorithm. The second column demonstrated the smoother results of the proposed algorithm. The fourth column represents the images acquired by

scans, and the sensitivity, specificity and accuracy of carotid atherosclerosis detection was 0.71, 0.85 and 0.80 respectively.

TABLE II. THE RESULTS OF DETECTION TEST FOR 2D IMAGES

Labels	Predictions	
	Positive (plaque)	Negative
Positive (plaque)	454	171
Negative	50	1687

TABLE III. THE DETECTION RESULTS OF CA FOR SCANS

Labels	Predictions	
	Positive (plaque)	Negative
Positive (plaque)	25	10
Negative	10	57

B. Reconstruction and Reprojection Accuracy

Fig. 8 illustrated three representative examples of the longitudinal images without regularization, with regularization clinical US images acquired by experienced sonographers, and the corresponding orientation information. The results revealed that the regularized reconstructed volume was smoother with less image artifacts. Fig. 9 demonstrated an example with large fallback of trajectory, the results showed there were still artifacts if directly apply the regularized algorithm and the proposed re-rank algorithm could remove the reconstruction artifacts. Fig. 10 illustrated the 3D volumes reconstructed from the auto-segmentation and ground truth respectively. The volumes were rendered by 3D-slicer (www.slicer.org). The

results showed that the segmentation module achieved good agreement with human label. Furthermore, the sunken of the lumen area indicated the existence of the plaque. Fig. 11

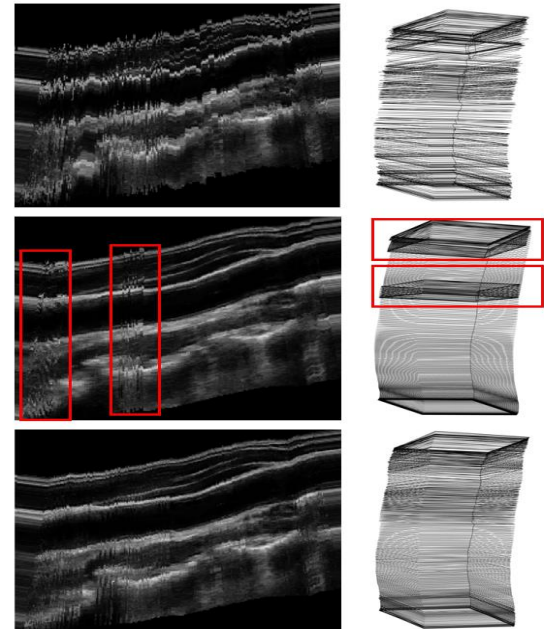


Fig. 9. Illustration of the proposed re-rank algorithm, the first row demonstrated the longitudinal image and corresponding position information without regularized algorithm. The second row represented the images which applied regularized algorithm and the third row showed the images which used re-rank and regularized algorithm.

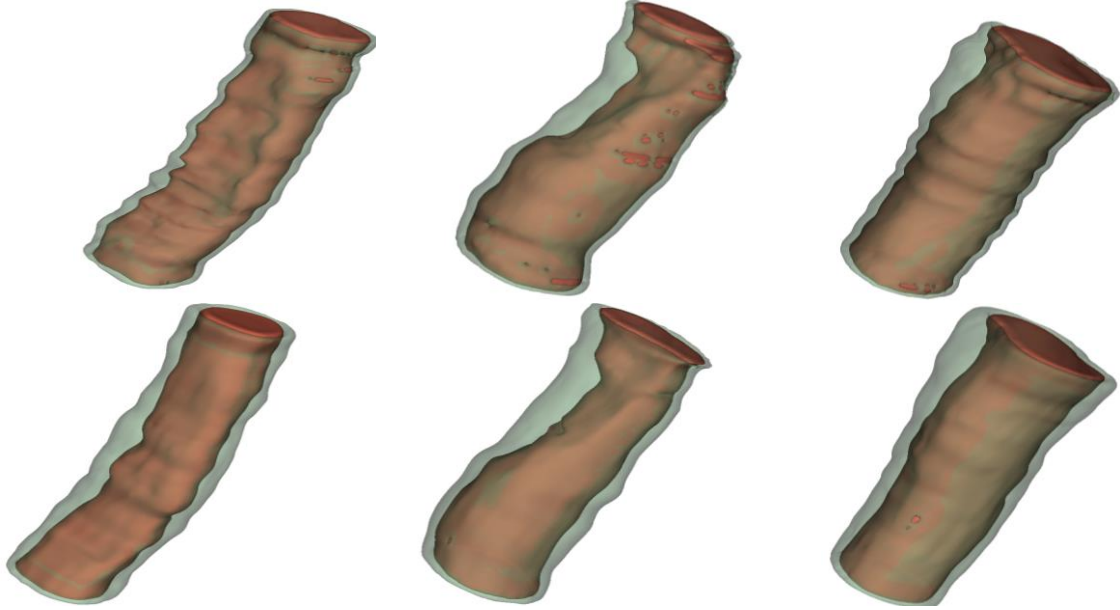


Fig. 10. The 3D volumes from the auto-segmentation (the first row) and ground truth (the second row). The translucent outer wall represents the vessel wall area, the inside red 3D volume represents the lumen area. The sunken of the lumen area indicated the existence of the plaque. The resolution of reconstruction is set to $0.2 \times 0.2 \times 0.2 \text{ mm}^3$.

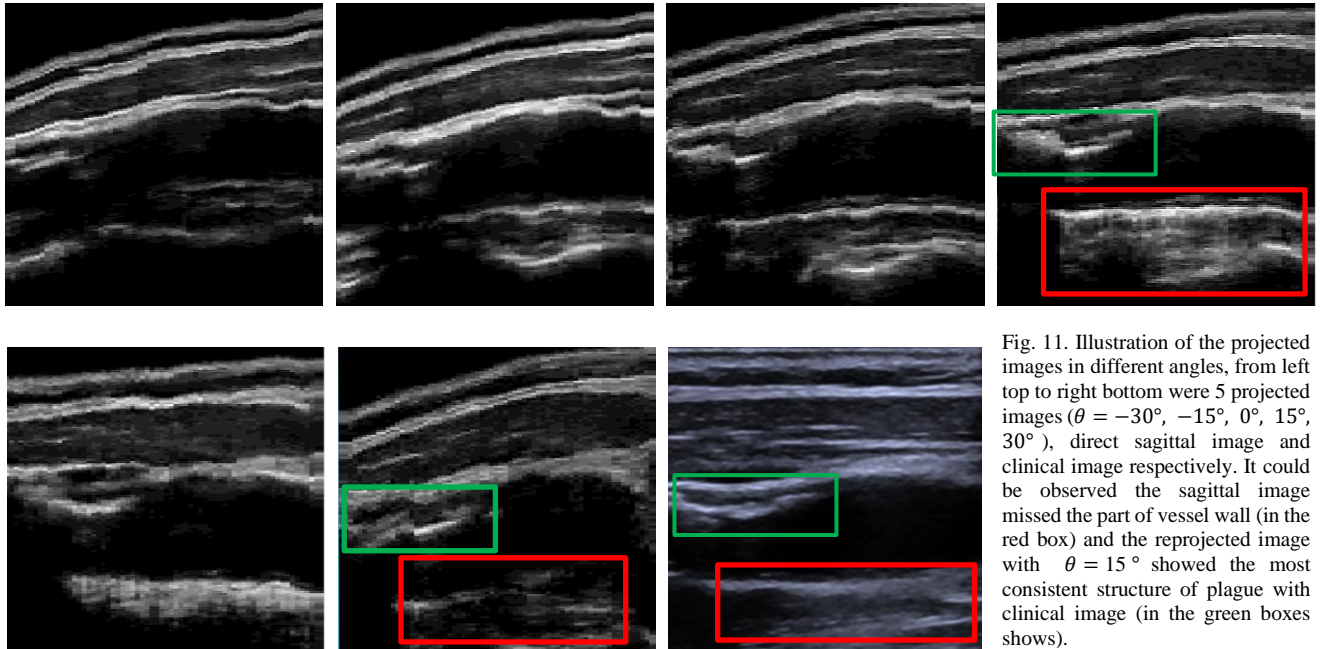


Fig. 11. Illustration of the projected images in different angles, from left top to right bottom were 5 projected images ($\theta = -30^\circ, -15^\circ, 0^\circ, 15^\circ, 30^\circ$), direct sagittal image and clinical image respectively. It could be observed the sagittal image missed the part of vessel wall (in the red box) and the reprojected image with $\theta = 15^\circ$ showed the most consistent structure of plaque with clinical image (in the green boxes shows).

demonstrated comparison among 5 projected images in different angles ($\theta = -30^\circ, -15^\circ, 0^\circ, 15^\circ, 30^\circ$), the image directly projected to sagittal plane and the manually acquired image by expert from the same atherosclerosis patient. The results showed that the projected images in different angles could reveal more structures of the carotid than the images only projected to sagittal plane. On the other hand, in Fig. 11, the image in 15° projection angle was most consistent with the clinical image obtained by expert using clinical US device, which indicated that the reprojection of 3D volume could simulate the different scan angles operated by expert to locate the best observation view.

The plaque size (length and thickness) measured from the pseudo volume, reconstructed volume and images acquired by expert were compared in Table IV. The results showed good agreement between the automatic measurement from the reconstructed volume and the manual method, while the plaque size measured by pseudo volume showed large difference with the expert measurement. The results indicated that the 3D reconstruction could reveal the true geometry and clinical metric of the carotid artery.

TABLE IV. MAD MEASUREMENTS (N=20) BETWEEN CLINICAL US DEVICE AND THE PROPOSED TECHNIQUES

	Plaque length(mm)	Plaque thickness(mm)	Plaque length (relative error)	Plaque thickness (relative error)
3D Reconstructed volume	2.65±2.36	0.842±0.617	15.4%±13.6%	26.0%±13.2%
Direct stacked Pesudo volume	6.54±7.23	0.976±0.648	40.0%±48.0%	29.4%±14.0%

C. Stenosis Measurement Accuracy

Fig. 12 demonstrated the linear correlation ($r=0.762$) of the stenosis grade measured by the system and experienced sonographers using the clinical US device on 20 carotid atherosclerosis patients, which indicated the proposed technique had the strong consistency with expert manual approach in carotid atherosclerosis diagnosis.

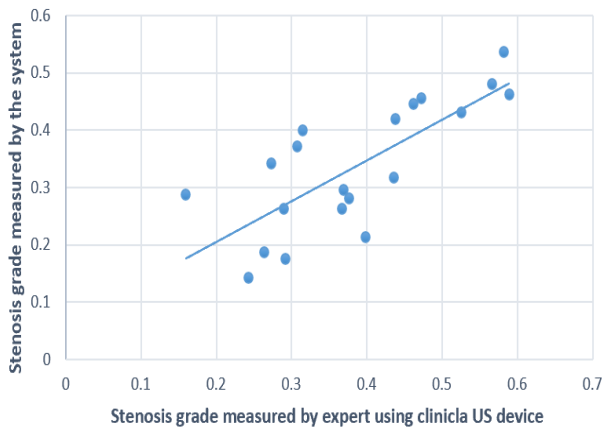


Fig. 12. correlation of stenosis grade between the manual measurement by expert using the clinical US device and the automatic measurement from the proposed technique on 20 carotid atherosclerosis patients.

V. DISCUSSION

In this study, we proposed a portable freehand 3D US imaging technique for carotid artery diagnosis which could achieve real 3D geometry of carotid artery, and the method showed good agreements with manual measurement of stenosis rate and classification of diseased and healthy case. The system was transportable and less dependent on operator's experience, which make it possible for routine health check in different environments such as community or rural area. In addition, the 3D reconstructed geometry could provide visualized carotid artery structure for further atherosclerosis evaluation.

Since the large position variation or fallback movement during scan would cause reconstruction artifacts, we designed a standard scan protocol for 3D carotid US data acquisition and analysis. The whole processing steps included automatic 3D US data acquisition, MAB and LIB segmentation, 3D reconstruction, automatic classification and measurement. In practice, the intermediate results of each step could be reviewed and manually corrected by operator if necessary to ensure the accurate final results. The diagnosis result was based on two key points: one was the accurate segmentation of vessel area, and the other was the correct reconstruction volume. The segmentation determined the region of interest (ROI) used for

following analysis including automatic stenosis evaluation, plaque size measurement and 3D geometry visualization. The wrong mask might crop regions out of the carotid artery, mislead the diagnosis network and cause confusing diagnosis results. However, if the 3D volume was directly reconstructed from original 2D frames before segmentation, the reconstruction artifacts around MAB and LIB such as misplacement or severe blurring could lead to segmentation error of vessels, especially for some cases with large position variation as Fig. 13. showed. Therefore, we conducted segmentation on the original 2D US image sequence before 3D reconstruction to extract the vessel area firstly to reduce the influence of reconstruction artifacts.

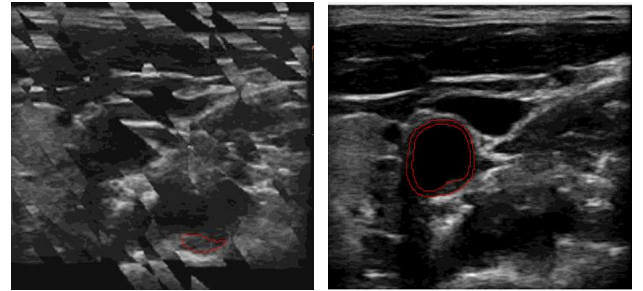


Fig. 13. Segmentation results on a transverse image collected from the 3D volume reconstructed by the original image sequence (left) and on an original transverse frame data (right). It could be observed that the severe artifacts on the left image led to wrong segmentation result.

For the reconstruction process, the failure reconstruction caused by large position variation could result in severe image artifacts which totally deviated the structure of the carotid artery as shown in Fig. 14. For the freehand US scan, theoretically, the position information recorded by magnetic sensor would be consistent with US probe motion i.e., the position of every US

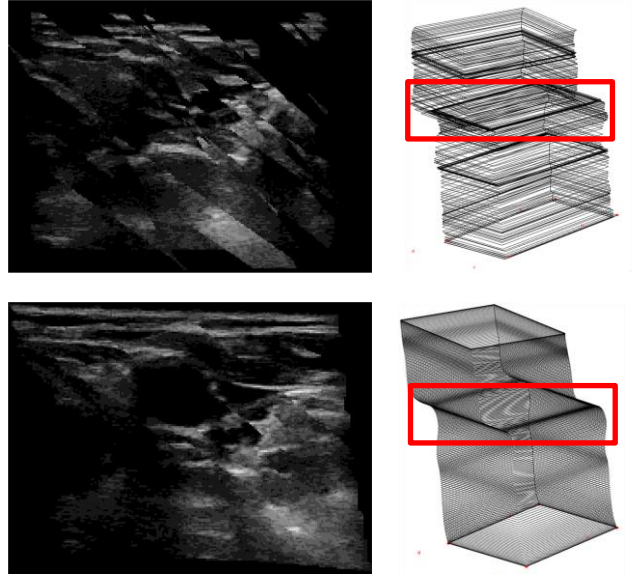


Fig. 14. Severe reconstruction artifacts caused by the large position variation. The image in first row represented the reconstructed volume and the orientation information with regularized algorithm while the images in the second row represented the results without regularized algorithm. The left image shows the transverse image of the locations in the reconstructed volume marked in red boxes in the right image, the large distortion could be observed in the image while the distortion was alleviated using the regularized algorithm.

image. However, the low precision of the sensor and inevitable hand jitter would lead to the noticeable measurement uncertainty of the position information along the scan direction and influence the reconstruction accuracy. Therefore, we adopted a novel total variation regularization algorithm to smooth the track of the position information and decrease distortion and disconnection of the image volume. The position of the freehand scan can be regarded as continuous and sequential array; therefore, the proposed regularization algorithm could reduce the uncertainty by constructing and minimize a regularized formulate in the manifold of Euclidean transformations. Meanwhile, a re-rank strategy was designed to solve the unordered image sequence caused by fallback movement during scan. In the future, the reconstruction accuracy could be further improved using the neural network.

After segmentation and reconstruction, the carotid artery volume could be obtained for further analysis such as healthy or diseased case diagnosis, plaque thickness, length area measurement, plaque type identification and stenosis measurement etc. In the diagnosis module, the cropped and resized images instead of the whole US images were used as the input. Since the plaque was only located inside vessel wall area, removing useless information outside the vessel wall could accelerate network training and improve the detection accuracy. On the other hand, there may be low intensity area in the vessel region which could mislead the network and result in wrong classification since negative sample (no plaque) usually had low intensity in lumen area. Therefore, the MAB and LIB mask were introduced to combine the morphological information with original image information to improve the detection accuracy. However, the proposed approach just utilized the consecutive 2D reconstructed transverse US images to detect plaque cases, thus some cases with small plaque size or severe artifacts were wrongly classified as no plaque. In the future, we will take the z axis information into account and use the whole 3D volume as input instead of detecting plaque by limited consecutive transverse slices to improve the accuracy of the diagnosis module.

We utilized a reprojection algorithm to project the carotid artery volume to longitudinal planes, so that the clinical metric such plaque length, thickness could be directly measured from the 3D volume with no need of new acquisition in sagittal direction. The traditional clinical carotid artery US examination required appropriate positioning and angle between transducer and neck, which greatly relies on the operator's experience to localize the plaque and obtain a high-quality US image, the proposed reprojection approach in our method was not only relatively convenient but could reveal the complete structure of the carotid artery with only one scan, and the images obtained by our automatic method achieved great agreement with the images obtained by expert using clinical US device.

In segmentation module, we used U-Net to segment the MAB and LIB in 2D US image sequence. Every image in the sequence was treated as a single image for the segmentation network. However, this approach didn't exploit the context information in the adjacent frames. In addition, some cases with severe noise or shadowing would result in wrong segmentation as Fig. 15 showed. In the future, 3D convolution will be considered to correct the segmentation mistake by utilizing the context information of the adjacent frames, and sample size will

be enlarged to improve the accuracy and robustness of the segmentation algorithm. More 3D metrics such total plaque volume, vessel wall volume, etc. would be evaluated for more accurate validation. On the other hand, the learning-based 3D reconstruction algorithm would be taken into account to improve the performance of reconstruction.

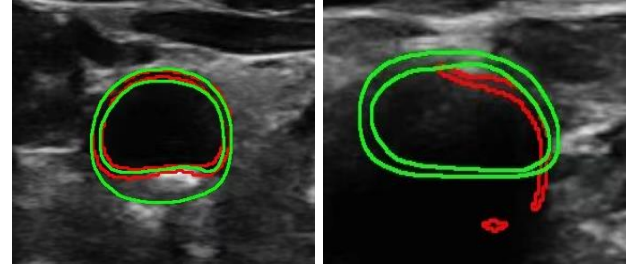


Fig. 15. Two representative wrong segmentation examples. The red line represented the automatic segmentation results by the segmentation module and the green line represented the human labels. The plaque was identified as the adventitia in the first case. In the second case, the vessel wall structure was disappeared and the segmentation network resulted in wrong segmentation.

VI. CONCLUSION

We have proposed an automatic 3D carotid artery imaging and diagnosis technique specially designed for the portable freehand ultrasound device. The technique applied a novel 3D reconstructed algorithm and a robust segmentation algorithm for automatic carotid atherosclerosis analysis. The results demonstrated that the technique achieved good agreement with manual expert examination on plaque diagnosis and stenosis grade measurement, which showed the potential application on fast carotid atherosclerosis examination and the follow-ups, especially for those scenarios where professional medical device and experienced clinicians are hard to acquire such as rural area or community with large population.

ACKNOWLEDGEMENT

This work was sponsored by Natural Science Foundation of China (NSFC) under Grant No.12074258.

REFERENCES

- [1] M. L. Flaherty *et al.*, "Carotid artery stenosis as a cause of stroke," *Neuroepidemiology*, vol. 40, no. 1, pp. 36–41, 2013.
- [2] L.-Y. Ma *et al.*, "China cardiovascular diseases report 2018: an updated summary," *J. Geriatr. Cardiol. JGC*, vol. 17, no. 1, p. 1, 2020.
- [3] H. R. Underhill, T. S. Hatsukami, Z. A. Fayad, V. Fuster, and C. Yuan, "MRI of carotid atherosclerosis: clinical implications and future directions," *Nat. Rev. Cardiol.*, vol. 7, no. 3, pp. 165–173, 2010.
- [4] M. Wintermark *et al.*, "High-resolution CT imaging of carotid artery atherosclerotic plaques," *Am. J. Neuroradiol.*, vol. 29, no. 5, pp. 875–882, 2008.
- [5] P. J. Nederkoorn, Y. van der Graaf, and M. M. Hunink, "Duplex ultrasound and magnetic resonance angiography compared with digital subtraction angiography in carotid artery stenosis: a systematic review," *Stroke*, vol. 34, no. 5, pp. 1324–1331, 2003.
- [6] Y. Inaba, J. A. Chen, and S. R. Bergmann, "Carotid plaque, compared with carotid intima-media thickness, more accurately predicts coronary artery disease events: a meta-analysis," *Atherosclerosis*, vol. 220, no. 1, pp. 128–133, 2012.
- [7] M. W. Lorenz, H. S. Markus, M. L. Bots, M. Rosvall, and M. Sitzer, "Prediction of clinical cardiovascular events with carotid intima-

media thickness: a systematic review and meta-analysis," *Circulation*, vol. 115, no. 4, pp. 459–467, 2007.

[8] A. Fenster, G. Parraga, and J. Bax, "Three-dimensional ultrasound scanning," *Interface Focus*, vol. 1, no. 4, pp. 503–519, 2011.

[9] T. Wannarong *et al.*, "Progression of carotid plaque volume predicts cardiovascular events," *Stroke*, vol. 44, no. 7, pp. 1859–1865, 2013.

[10] A. Fenster, C. Blake, I. Gyakos, A. Landry, and J. Spence, "3D ultrasound analysis of carotid plaque volume and surface morphology," *Ultrasound*, vol. 44, pp. e153–e157, 2006.

[11] G. C. Makris, A. Lavida, M. Griffin, G. Geroulakos, and A. N. Nicolaides, "Three-dimensional ultrasound imaging for the evaluation of carotid atherosclerosis," *Atherosclerosis*, vol. 219, no. 2, pp. 377–383, 2011.

[12] K. AlMuhanna *et al.*, "Carotid plaque morphometric assessment with three-dimensional ultrasound imaging," *J. Vasc. Surg.*, vol. 61, no. 3, pp. 690–697, 2015.

[13] R. M. Botnar, M. Stuber, K. V. Kissinger, W. Y. Kim, E. Spuentrup, and W. J. Manning, "Noninvasive coronary vessel wall and plaque imaging with magnetic resonance imaging," *Circulation*, vol. 102, no. 21, pp. 2582–2587, 2000.

[14] M. Herder, S. H. Johnsen, K. A. Arntzen, and E. B. Mathiesen, "Risk factors for progression of carotid intima-media thickness and total plaque area: a 13-year follow-up study: the Tromsø Study," *Stroke*, vol. 43, no. 7, pp. 1818–1823, 2012.

[15] B. Chiu, M. Egger, J. D. Spence, G. Parraga, and A. Fenster, "Quantification of carotid vessel wall and plaque thickness change using 3D ultrasound images," *Med. Phys.*, vol. 35, no. 8, pp. 3691–3710, 2008.

[16] X. Yang, J. Jin, W. He, M. Yuchi, and M. Ding, "Segmentation of the common carotid artery with active shape models from 3D ultrasound images," in *Medical Imaging 2012: Computer-Aided Diagnosis*, 2012, vol. 8315, p. 83152H.

[17] A. M. A. Lorza *et al.*, "Carotid artery lumen segmentation in 3D freehand ultrasound images using surface graph cuts," in *International conference on medical image computing and computer-assisted intervention*, 2013, pp. 542–549.

[18] J. de Ruijter, M. van Sambeek, F. van de Vosse, and R. Lopata, "Automated 3D geometry segmentation of the healthy and diseased carotid artery in free-hand, probe tracked ultrasound images," *Med. Phys.*, vol. 47, no. 3, pp. 1034–1047, 2020.

[19] M. Jiang, J. D. Spence, and B. Chiu, "Segmentation of 3D ultrasound carotid vessel wall using U-Net and segmentation average network," in *2020 42nd Annual International Conference of the IEEE Engineering in Medicine & Biology Society (EMBC)*, 2020, pp. 2043–2046.

[20] R. Zhou, A. Fenster, Y. Xia, J. D. Spence, and M. Ding, "Deep learning-based carotid media-adventitia and lumen-intima boundary segmentation from three-dimensional ultrasound images," *Med. Phys.*, vol. 46, no. 7, pp. 3180–3193, 2019.

[21] J. De Ruijter, J. J. Muijsers, F. N. Van de Vosse, M. R. Van Sambeek, and R. G. Lopata, "A generalized approach for automatic 3-D geometry assessment of blood vessels in transverse ultrasound images using convolutional neural networks," *IEEE Trans. Ultrason. Ferroelectr. Freq. Control*, vol. 68, no. 11, pp. 3326–3335, 2021.

[22] L. van Knippenberg, R. J. van Sloun, M. Mischi, J. de Ruijter, R. Lopata, and R. A. Bouwman, "Unsupervised domain adaptation method for segmenting cross-sectional CCA images," *Comput. Methods Programs Biomed.*, vol. 225, p. 107037, 2022.

[23] C. Azzopardi, K. P. Camilleri, and Y. A. Hicks, "Bimodal automated carotid ultrasound segmentation using geometrically constrained deep neural networks," *IEEE J. Biomed. Health Inform.*, vol. 24, no. 4, pp. 1004–1015, 2020.

[24] R. Zhou *et al.*, "A voxel-based fully convolution network and continuous max-flow for carotid vessel-wall-volume segmentation from 3D ultrasound images," *IEEE Trans. Med. Imaging*, vol. 39, no. 9, pp. 2844–2855, 2020.

[25] R. Zhou *et al.*, "Deep learning-based measurement of total plaque area in B-mode ultrasound images," *IEEE J. Biomed. Health Inform.*, vol. 25, no. 8, pp. 2967–2977, 2021.

[26] R. Zhou *et al.*, "Deep learning-based carotid plaque segmentation from B-mode ultrasound images," *Ultrasound Med. Biol.*, vol. 47, no. 9, pp. 2723–2733, 2021.

[27] Y. Xia, X. Cheng, A. Fenster, and M. Ding, "Automatic classification of carotid ultrasound images based on convolutional neural network," in *Medical Imaging 2020: Computer-Aided Diagnosis*, 2020, vol. 11314, p. 1131441.

[28] W. Ma *et al.*, "Multilevel strip pooling-based convolutional neural network for the classification of carotid plaque echogenicity," *Comput. Math. Methods Med.*, vol. 2021, 2021.

[29] H. Shen, W. Zhang, H. Wang, G. Ding, and J. Xie, "NDDR-LCS: A Multi-Task Learning Method for Classification of Carotid Plaques," in *2020 IEEE International Conference on Image Processing (ICIP)*, 2020, pp. 2461–2465.

[30] Y. Zhao, J. D. Spence, and B. Chiu, "Three-dimensional ultrasound assessment of effects of therapies on carotid atherosclerosis using vessel wall thickness maps," *Ultrasound Med. Biol.*, vol. 47, no. 9, pp. 2502–2513, 2021.

[31] R. Zhou, W. Ma, A. Fenster, and M. Ding, "U-Net based automatic carotid plaque segmentation from 3D ultrasound images," in *Medical Imaging 2019: Computer-Aided Diagnosis*, 2019, vol. 10950, pp. 1119–1125.

[32] L. Saba *et al.*, "Ultrasound-based carotid stenosis measurement and risk stratification in diabetic cohort: a deep learning paradigm," *Cardiovasc. Diagn. Ther.*, vol. 9, no. 5, p. 439, 2019.

[33] M. Biswas *et al.*, "Two-stage artificial intelligence model for jointly measurement of atherosclerotic wall thickness and plaque burden in carotid ultrasound: A screening tool for cardiovascular/stroke risk assessment," *Comput. Biol. Med.*, vol. 123, p. 103847, 2020.

[34] T. Wen *et al.*, "An accurate and effective FMM-based approach for freehand 3D ultrasound reconstruction," *Biomed. Signal Process. Control*, vol. 8, no. 6, pp. 645–656, 2013.

[35] O. V. Solberg, F. Lindseth, H. Torp, R. E. Blake, and T. A. N. Hernes, "Freehand 3D ultrasound reconstruction algorithms—a review," *Ultrasound Med. Biol.*, vol. 33, no. 7, pp. 991–1009, 2007.

[36] H. R. Roth *et al.*, "A new 2.5 D representation for lymph node detection using random sets of deep convolutional neural network observations," in *International conference on medical image computing and computer-assisted intervention*, 2014, pp. 520–527.

[37] D.-H. Lee and others, "Pseudo-label: The simple and efficient semi-supervised learning method for deep neural networks," in *Workshop on challenges in representation learning, ICML*, 2013, vol. 3, no. 2, p. 896.

[38] O. Ronneberger, P. Fischer, and T. Brox, "U-net: Convolutional networks for biomedical image segmentation," in *International Conference on Medical image computing and computer-assisted intervention*, 2015, pp. 234–241.

[39] H.-B. Chen, R. Zheng, L.-Y. Qian, F.-Y. Liu, S. Song, and H.-Y. Zeng, "Improvement of 3-D Ultrasound Spine Imaging Technique Using Fast Reconstruction Algorithm," *IEEE Trans. Ultrason. Ferroelectr. Freq. Control*, vol. 68, no. 10, pp. 3104–3113, 2021.

[40] S. Song, Y. Huang, J. Li, M. Chen, and R. Zheng, "Development of Implicit Representation Method for Freehand 3D Ultrasound Image Reconstruction of Carotid Vessel," in *2022 IEEE International Ultrasonics Symposium (IUS)*, 2022, pp. 1–4.

[41] M. Esposito *et al.*, "Total variation regularization of pose signals with an application to 3D freehand ultrasound," *IEEE Trans. Med. Imaging*, vol. 38, no. 10, pp. 2245–2258, 2019.

[42] J. Wu *et al.*, "Deep morphology aided diagnosis network for segmentation of carotid artery vessel wall and diagnosis of carotid atherosclerosis on black-blood vessel wall MRI," *Med. Phys.*, vol. 46, no. 12, pp. 5544–5561, 2019.

[43] H. Chen, R. Zheng, E. Lou, and L. H. Le, "Compact and Wireless Freehand 3D Ultrasound Real-time Spine Imaging System: A pilot study," in *Annual International Conference of the IEEE Engineering in Medicine and Biology Society. IEEE Engineering in Medicine and Biology Society. Annual International Conference*, 2020, vol. 2020, pp. 2105–2108.